Nonlocal modulation of the energy cascade in broadband-forced turbulence

Arkadiusz K. Kuczaj* and Bernard J. Geurts†
Multiscale Modeling and Simulation, J.M. Burgers Center for Fluid Dynamics, NACM, Department of Applied Mathematics, University of Twente, P.O. Box 217, 7500 AE Enschede, the Netherlands

W. David McComb
School of Physics, University of Edinburgh, James Clerk Maxwell Building, Mayfield Road, Edinburgh EH9 3JZ, United Kingdom
(Received 17 April 2006; published 31 July 2006)

Classically, large-scale forced turbulence is characterized by a transfer of energy from large to small scales via nonlinear interactions. We have investigated the changes in this energy transfer process in *broadband* forced turbulence where an additional perturbation of flow at smaller scales is introduced. The modulation of the energy dynamics via the introduction of forcing at smaller scales occurs not only in the forced region but also in a broad range of length scales outside the forced bands due to nonlocal triad interactions. Broadband forcing changes the energy distribution and energy transfer function in a characteristic manner leading to a significant modulation of the turbulence. We studied the changes in this transfer of energy when changing the strength and location of the small-scale forcing support. The energy content in the larger scales was observed to decrease, while the energy transport power for scales in between the large and small scale forcing regions was enhanced. This was investigated further in terms of the detailed transfer function between the triad contributions and observing the long-time statistics of the flow. The energy is transferred toward smaller scales not only by wave numbers of similar size as in the case of large-scale forced turbulence, but by a much wider extent of scales that can be externally controlled.

DOI: 10.1103/PhysRevE.74.016306 PACS number(s): 47.27.E−, 47.27.Gs, 47.27.Rc

I. INTRODUCTION

The dynamics of kinetic energy plays a central role in turbulent flows. The nonlinear term in the Navier-Stokes equations is responsible for the transfer of energy between any three wave vectors that form a triad in spectral space [1]. Along with the viscous and forcing terms this controls the production, transfer, and dissipation of energy in the system. The triadic interactions have been studied for decaying and forced turbulence by many authors (for a review, see Ref. [2]). Throughout the years various types of large-scale forcing methods [3–11] have been proposed to sustain quasistationarity in numerical turbulence as an idealized form of turbulent flow. The aim of such numerical experiments was to investigate the basic concept of the Kolmogorov (K41) theory [12] that proposes an inertial range in the kinetic energy spectrum and local transfer of energy within this range. The turbulent kinetic energy is on average transferred locally from larger to neighboring smaller scales.

The purpose of this paper is to numerically investigate the processes associated with the flow of energy in a turbulent flow. Specifically, we consider *modulated* turbulence in which the modifications involve the supplementary forcing in a wide range of modes located in an inertial range of the flow. In the literature, mainly turbulence with forcing restricted to the large scales has been examined in detail [2]. The small scale behavior was found to be energetically quite insensitive to the type of forcing and at sufficiently high Reynolds numbers a well-developed inertial range was observed [13]. Against this background, we extend the use of forcing methods and investigate their application directly in the inertial range, thereby focusing particularly on the competition between transfer and forcing. We quantify the dominant alterations due to the broadband forcing in terms of changes in the energy cascading processes. We pay attention to the energy transfer function and consider changes that arise in the contributions from "local," 'nonlocal," and "distant" triadic interactions. Compared to traditional large-scale forced turbulence, we observe a strengthening of the contributions of nonlocal interactions, leading to a modification of the inertial range spectrum.

High-resolution direct numerical simulations of turbulence that measure the influence of individual terms in the Navier-Stokes equations on the triadic interactions have been reported [14–20]. It was found that the energetically dominant triadic interactions involve sets of three modes in which the magnitude of the wave vector of one of the modes differs considerably from the other two. This suggests that statistics of smaller scales may be affected by larger scales. These dominant processes are not in contradiction with the Kolmogorov theory because the energy is mainly exchanged between the two modes of quite similar wave-vector size [19]. Only a small net energy transfer toward larger wave numbers arises that involves a detailed cancellation between many individual triad transfers [20]. The spectral space dynamics is characterized by a multitude of separate transfer processes among various modes. These contributions can be collected in pairs with opposite sign and almost the same magnitude. In total, this leads to a large number of "near cancellations" and hence only a comparably small net effect remains that constitutes the well-known "downward cascading" toward

*Electronic address: a.k.kuczaj@utwente.nl
†Also at Anisotropic Turbulence, Fluid Dynamics Laboratory, Department of Applied Physics, P.O. Box 513, 5300 MB Eindhoven, The Netherlands.

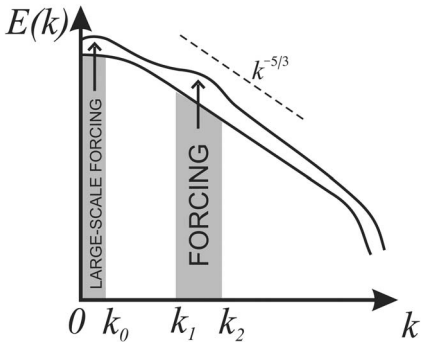

FIG. 1. Broadband forcing in spectral space. Large-scale forcing $k \leq k_0$ with an additional high-k forced region $k_1 < k \leq k_2$.

higher wave numbers in spectral space. This was confirmed with the use of helical mode decomposition in Ref. [20].

The dynamics of actual turbulent flows seen in nature is usually characterized by an enormous number of interacting scales, often perturbed by geometrically complex boundaries and influenced by additional forces such as rotation and buoyancy. This can lead to inhomogeneity and anisotropy, which are not covered directly in the classical view of the Kolmogorov energy cascade and may express themselves in nonlocal interactions of various particular scales of motion. The complexity of such systems motivated us to study in more detail forcing methods that simultaneously perturb a prescribed range of scales [21]. Such "broadband" agitation of various scales of motion is observed experimentally in turbulent drag reduction by fiber suspension [22,23], flows through porous media [24], and over tree canopies [25]. In these cases the energy is transferred abruptly to small scales when the flow reaches an obstruction. Various other types of flows also exhibit turbulent motions that coexist at different scales [26].

To explore the possibilities of a broader application of forcing methods in turbulence modeling and concurrently examine the energy dynamics in flows that do not directly follow the classical Kolmogorov $-5/3$ scaling we employ numerical simulations of *broadband* forced turbulence. The forcing studied in this paper represents a continual addition or removal of energy from a broad range of scales in the system, thereby providing the possibility of altering the characteristic $-5/3$ slope in the kinetic energy spectrum as predicted by the K41 theory. Specifically, as indicated in Fig. 1, we apply the forcing to two regions. The large-scale forcing $k \leq k_0$ classically agitates the largest scales in a flow while the additional band $k_1 < k \leq k_2$ is located in a region of the inertial regime, to allow a direct competition with the nonlinear transfer term. For inertial-range scales broadband forcing introduces explicit energy injection next to the transfer term. We varied the spectral support and strength of the high-k band to investigate the modulation of the turbulence that develops. This distinguishes it from the classical forcing of large scales only.

In this paper we compute changes in the energy distribution associated with the broadband forcing and observe a characteristic alteration in the spectral energy transfer compared to the classical Kolmogorov cascading. This alteration expresses itself by additional local minima and maxima in the transfer function. It is well known that in cases with large-scale forcing only, negative values are found for the transfer at the smallest wave numbers indicating the energy injection at these scales. The positive values for the transfer that arise for all other wave numbers indicates the energy cascading process to smaller scales. In our case of broadband forcing in the inertial range, additional negative regions appear in the transfer function. These coincide with the additional local injection of energy. Such a negative region is bordered by nearby additional maxima in the transfer. These characterize the associated increased energy transfer to scales just larger or just smaller than the broadband forced region.

Forcing applied to different spatial scales simultaneously allows a nonlocal modulation of the energy distribution compared to the reference Kolmogorov case. To quantify the alterations in the energy transfer we use a decomposition of the velocity field closely following Ref. [16] and investigate the magnitude of the contributions from various spatial scales to the overall energy transfer.

The main finding of this study pertains to the role of broadband inertial range forcing in modifying the natural energy cascading process. This is understood explicitly in terms of changes in the detailed nonlocal energy transfer. In addition, we illustrate and quantify the mechanism of enhancement of the total energy transfer to smaller scales arising from broadband forcing and the depletion of the energy content in the large scales. Agitation of certain high wave numbers can affect well separated low wave number components in a flow. These findings may be relevant for problems that involve the control of turbulent flow in complex geometries in which various scales of motions are simultaneously agitated, e.g., in compact heat exchangers [24]. Further applications of such broadband forcing may be connected with the observed modulations of transport properties in physical space leading to an enhanced scalar dispersion rate [21].

The organization of this paper is as follows. The mathematical formulation of the problem is given in Sec. II, where the computational method and the energy transfer terms are also described. The energy spectra of broadband forced turbulence and the modulation of the energy transfer are investigated in Sec. III. In Sec. IV we present a more detailed view of the energy transfer processes by computing partitioned energy transfer function over various spatial scales. The paper closes with a summary in Sec. V.

II. COMPUTATIONAL FLOW MODEL

A. Equations of motion

The incompressible Navier-Stokes equations in spectral (Fourier) representation can be written as

$$(\partial_t + \nu k^2) u_\alpha(\mathbf{k},t) = \Psi_\alpha(\mathbf{k},t) + F_\alpha(\mathbf{k},t), \tag{1}$$

where $u_\alpha(\mathbf{k},t)$ is the velocity field coefficient at wave vector $\mathbf{k}$ ($k=|\mathbf{k}|$) and time t [1]. The nondimensional kinematic viscosity ν is the inverse of the computational Reynolds number ($\mathrm{Re}=1/\nu$). The nonlinear term reads

$$\Psi_\alpha(\mathbf{k},t) = M_{\alpha\beta\gamma} \sum_{\mathbf{p}+\mathbf{q}=\mathbf{k}} u_\beta(\mathbf{p},t) u_\gamma(\mathbf{q},t), \tag{2}$$

and the forcing term $F_\alpha(\mathbf{k},t)$ is specified in Sec. II B. The tensor $M_{\alpha\beta\gamma}$ in Eq. (2) accounts for the pressure and incompressibility effects:

$$M_{\alpha\beta\gamma} = \frac{1}{21}(k_\beta D_{\alpha\gamma} + k_\gamma D_{\alpha\beta}), \tag{3}$$

in which

$$D_{\alpha\beta} = \delta_{\alpha\beta} - k_\alpha k_\beta / k^2. \tag{4}$$

Taking the inner product of (1) and $u^*_\alpha(\mathbf{k},t)$, where the asterisk denotes the complex conjugate, we obtain the energy equation

$$(\partial_t + 2\nu k^2) E(\mathbf{k},t) = T(\mathbf{k},t) + T_F(\mathbf{k},t). \tag{5}$$

The spectral energy density is denoted by $E(\mathbf{k},t) = \frac{1}{2} u^*_\alpha(\mathbf{k},t) u_\alpha(\mathbf{k},t)$. The rate of energy exchanged at wave vector $\mathbf{k}$ with all other modes in the system is characterized by the energy transfer function

$$T(\mathbf{k},t) = u^*_\alpha(\mathbf{k},t) \Psi_\alpha(\mathbf{k},t). \tag{6}$$

The rate of energy provided by the forcing term is

$$T_F(\mathbf{k},t) = u^*_\alpha(\mathbf{k},t) F_\alpha(\mathbf{k},t), \tag{7}$$

and the energy dissipation rate present in Eq. (5) reads

$$\varepsilon(\mathbf{k},t) = 2\nu k^2 E(\mathbf{k},t). \tag{8}$$

The three terms $T(\mathbf{k},t)$, $T_F(\mathbf{k},t)$ and $\varepsilon(\mathbf{k},t)$ represent the energy dynamics in the system that each typically act in distinct wave-number regions. The forcing term $T_F(\mathbf{k},t)$ is nonzero in the forced modes only. In this paper the collection of forced modes will always contain a low wave-number band corresponding to large-scale forcing of the flow. In addition, higher wave-number contributions will be included in $T_F(\mathbf{k},t)$. In contrast, the energy dissipation rate $\varepsilon(\mathbf{k},t)$ is defined in the entire spectral space, but it is dynamically important primarily for the high wave-number range. Finally, the transfer term $T(\mathbf{k},t)$ is basic to the development of an energy cascade and is a dominant contribution for wave numbers in an inertial range [1].

The change of the total energy $\hat{E}$ in the system is connected with its viscous dissipation and the total effect of the forcing. In fact, introducing

$$\hat{E}(t) = \sum_{\mathbf{k}} E(\mathbf{k},t), \tag{9}$$

we find

$$\partial_t \hat{E}(t) = \hat{T}_F(t) - \hat{\varepsilon}(t), \tag{10}$$

where $\hat{\varepsilon}(t) = \Sigma_{\mathbf{k}} \varepsilon(\mathbf{k},t)$ and $\hat{T}_F(t) = \Sigma_{\mathbf{k}} T_F(\mathbf{k},t)$. We used the fact that the total energy transfer $\hat{T}(t) = \Sigma_{\mathbf{k}} T(\mathbf{k},t) = 0$. The injection of energy occurs only in the forced region. This keeps the whole system in a quasistationary state. Normally, the forced region is restricted to the largest scales in a flow represented by the smallest wave numbers [5,10]. The energy introduced in the large scales is transferred to smaller scales and dissipated primarily in very localized flow features of viscous length scales. By the introduction of an additional source of energy in the inertial range we will study the perturbation of the energy cascading process by the forcing.

B. Forcing method

Forcing is achieved by applying an additional driving $F_\alpha(\mathbf{k},t)$ to the velocity field in Fourier space, cf. Eq. (1). Conventionally, the turbulent cascade develops as a statistical equilibrium is reached, characterized by the balance between the input of kinetic energy through the forcing and its removal through viscous dissipation. In literature [3–11], we may distinguish several numerical approaches to forced turbulence that all refer to the agitation of the largest scales of motion. Here, we modify such classical forcing procedures by allowing for the simultaneous agitation of a broader range of intermediate-k modes as depicted in Fig. 1.

We study two ranges of forcing: the classical large-scale forcing ($k \leq k_0$) and small-scale forcing localized in the spectral region where the transfer of energy $T(\mathbf{k},t)$ is important ($k_1 < k \leq k_2$). By narrowing or widening the width of the forced bands, along with a change in their location in spectral space we can control several aspects of the energy dynamics. The strength of forcing is controlled by the amount of energy introduced to various regions in spectral space.

We expect the small-scale forcing band to influence the interscale energy transfer process not only between scales of similar size but at a wider spectrum of scales. This may be understood globally as follows. The process of energy cascading is mainly interpreted via the resulting local transfer of energy in spectral space [19]. However, this total energy transfer results from many nonlocal contributions and these may be directly altered by the additional small-scale forcing. Correspondingly an influence on the overall energy cascading process may occur over an extended wave-number range. We quantify this effect by evaluating the nonlinear interactions among the various modes while they are being perturbed by the broadband forcing.

In this paper we adopt the recently proposed fractal forcing [27], which involves a power-law dependence of F_α on the wave number:

$$F_\alpha(\mathbf{k},t) = \tilde{\varepsilon}_w(\mathbf{k}) \frac{k^\beta e_\alpha(\mathbf{k},t)}{\sum_{\mathbf{k}\in\mathbb{K}} k^\beta \sqrt{2E(\mathbf{k},t)}}, \tag{11}$$

where the coefficient $\beta = D_f - 2$ is connected with the fractal dimension D_f of the stirrer and $\tilde{\varepsilon}_w(\mathbf{k})$ is the energy input rate at mode $\mathbf{k}$. The fractal forcing is based on a simple argument of drag enhancement associated with flow passing through complex "porous" regions, e.g., a metal foam or the canopy of a tree. The complexity of such obstructing objects may be captured to some extent in terms of their fractal dimension D_f as elaborated in literature (see, e.g., Refs. [25,27] and references therein). In Ref. [21] the effect of various deterministic forcing methods was compared and a qualitative independence of the particular type of forcing was observed, both in case of large-scale forcing only and when broad band

forcing was adopted. In this paper we selected the fractal forcing as a characteristic forcing procedure for further investigation of the nonlocal alterations in the energy transfer. The fractal dimension D_f is taken equal to 2.6, close to the experimental value found for fractal grids reported in Ref. [28]. Variation of D_f by about 20% was considered and found to yield only small effects on the spectrum.

The set of forced modes $\mathbb{K}$ is composed of bands $\mathbb{K}_{m,p}$ $(m \leq p)$ which consist of $p-m+1$ adjacent spherical shells $\mathbb{S}_n = \frac{2\pi}{L_b}(n-1/2) < |\mathbf{k}| \leq \frac{2\pi}{L_b}(n+1/2)$: $m \leq n \leq p$, in terms of the size of the computational domain denoted by L_b. In the simulations we always force the first shell $\mathbb{S}_1$ and a single high-k band $\mathbb{K}_{m,p}$, if not stated otherwise. The classical large-scale forcing of the first shell $\mathbb{S}_1$ has a constant energy injection rate $\varepsilon_{w,1}$ in Eq. (11) while $\mathbb{K}_{m,p}$ has a constant strength $\varepsilon_{w,2}$ and a support in spectral space controlled by m and p:

$$\tilde{\varepsilon}_w(\mathbf{k}) = \begin{cases} \varepsilon_{w,1} & \text{if } \mathbf{k} \in \mathbb{S}_1, \\ \varepsilon_{w,2} & \text{if } \mathbf{k} \in \mathbb{K}_{m,p}, \\ 0 & \text{otherwise}. \end{cases} \tag{12}$$

The vector $\mathbf{e}$ in Eq. (11) is given by [27]

$$\mathbf{e}(\mathbf{k},t) = \frac{\mathbf{u}(\mathbf{k},t)}{|\mathbf{u}(\mathbf{k},t)|} + 1\,\frac{\mathbf{k}\times\mathbf{u}(\mathbf{k},t)}{|\mathbf{k}||\mathbf{u}(\mathbf{k},t)|}. \tag{13}$$

This vector consists of two parts, either parallel or perpendicular to the vector $\mathbf{u}(\mathbf{k},t)$. In this forcing procedure, we have control over the energy input rate, the range of forced modes, and the effective geometrical complexity of the stirrer represented by the fractal dimension.

The summation over all forced modes of $u_\alpha^*(\mathbf{k},t)F_\alpha(\mathbf{k},t)$ yields a total energy input rate given by

$$\hat{T}_F(t) = \sum_{\mathbf{k}} T_F(\mathbf{k},t) = \sum_{\mathbf{k}} u_\alpha^*(\mathbf{k},t)F_\alpha(\mathbf{k},t) = \varepsilon_w, \tag{14}$$

where $\varepsilon_w = \varepsilon_{w,1} + \varepsilon_{w,2}$. The energy input leads to a quasistationary state described by the energy equation

$$\partial_t \hat{E}(t) = \varepsilon_w - \hat{\varepsilon}(t). \tag{15}$$

This characterizes the energy dynamics in the system at the most global level. We observe that this forcing implies a constant energy injection rate that results in a fluctuating total energy $\hat{E}$ and a fluctuating total energy dissipation rate with mean ε_w.

C. Energy transfer

A detailed investigation of the energy transfer in large-scale forced turbulence [19] shows that the dominant triadic interactions occur between wave vectors of quite different lengths. Hence large-scale forcing may be directly involved in the dynamics of much smaller scales [29]. The interactions are roughly classified as "local" when the sizes of all wave vectors in a triad are similar, "nonlocal" when the scale separation is about a factor 10–15 and "distant" when the separation is much larger [30]. It was shown that the transfer of energy reaches maximum values for triads with two wave vectors of similar size and one with quite different length

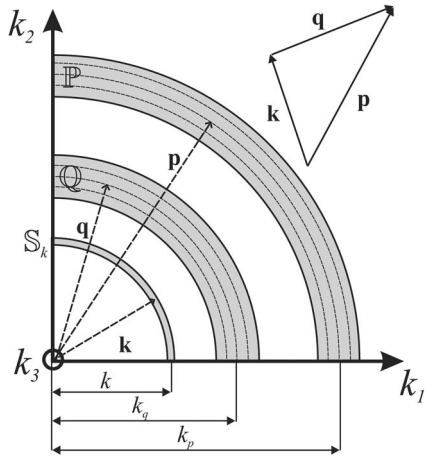

FIG. 2. Schematic triadic interaction that occurs between wave vector $\mathbf{k}$ in shell $\mathbb{S}_k$ and wave vectors $\mathbf{p}$, $\mathbf{q}$ taken from regions $\mathbb{P}$ and $\mathbb{Q}$ of spectral space that each consist of four shells with central wave numbers k_p and k_q.

[19]. Although, the interactions between triads can be seen mainly as nonlocal, the dominant net energy transfer is local, i.e., occurring between similar scales [13,31,32]. The interactions produce forward and backward energy transfer that combined result in a small net forward energy transfer because of the detailed balance between contributions that virtually cancel each other [20]. The forward cascade in the inertial range was found to be dominated by local and nonlocal interactions, while the distant interactions do not significantly transfer energy [30]. All these findings concern the classical turbulence forced at the largest scales.

Against this background, we ask what the turbulence response will be to a broadband perturbation of the energy transfer processes? In recent literature a somewhat related study was reported in Ref. [33]. Decaying turbulence that starts from an initial condition with an energetically strongly enhanced small-scale band of modes was studied. The presence of the extra small-scale band was found to reduce the intensity of the developing turbulence by enhancing the *nonlocal energy cascade* directly towards smaller scales. This removes the kinetic energy more efficiently. The energy feeding mechanisms and energy transfer also attract much attention in transitional and turbulent flows with an active control [34]. The modulation induced by the broadband forcing has its consequences, not only in the spectral space dynamics of a flow but also in its physical space transport properties [21].

To analyze the response of turbulence to the additional broadband perturbation in more detail we apply previously developed methods used in the examination of energy transfer in large-scale forced turbulence [16]. Referring to Fig. 2, the energy transfer between a wave vector $\mathbf{k}=(k_1,k_2,k_3)$ and all pairs of wave vectors $\mathbf{p}$ and $\mathbf{q}=\mathbf{k}-\mathbf{p}$ with $\mathbf{p}$, $\mathbf{q}$ chosen in some prescribed regions $\mathbb{P}$ and $\mathbb{Q}$ will be investigated. Such a decomposition allows measuring the contribution of separate scales to the transfer function $T(\mathbf{k},t)$. The precise specification requires a few steps that are presented next. First, we define the truncated velocity field as

$$u_\alpha^{(\mathbb{P},\mathbb{Q})}(\mathbf{k},t) = \begin{cases} u_\alpha(\mathbf{k},t) & \text{if } \mathbf{k} \in \mathbb{P} \text{ or } \mathbf{k} \in \mathbb{Q}, \\ 0 & \text{otherwise}. \end{cases} \tag{16}$$

Based on this truncated velocity field we may compute the energy transfer involving the wave vector $\mathbf{k}$ and all wave vectors $\mathbf{p}$ and $\mathbf{q}$:

$$T_{\mathbb{PQ}}(\mathbf{k},t) = \begin{cases} \tilde{T}_{\mathbb{PP}}(\mathbf{k},t) & \text{if } \mathbb{P} = \mathbb{Q}, \\ \frac{1}{2}[\tilde{T}_{\mathbb{PQ}}(\mathbf{k},t) - \tilde{T}_{\mathbb{PP}}(\mathbf{k},t) - \tilde{T}_{\mathbb{QQ}}(\mathbf{k},t)] & \text{if } \mathbb{P} \neq \mathbb{Q}, \end{cases} \tag{17}$$

where

$$\tilde{T}_{\mathbb{PQ}}(\mathbf{k},t) = u_\alpha^*(\mathbf{k},t)\Psi_\alpha^{(\mathbb{P},\mathbb{Q})}(\mathbf{k},t). \tag{18}$$

The nonlinear term $\Psi_\alpha^{(\mathbb{P},\mathbb{Q})}(\mathbf{k},t)$ is defined by the convolution of the truncated fields:

$$\Psi_\alpha^{(\mathbb{P},\mathbb{Q})}(\mathbf{k},t) = M_{\alpha\beta\gamma} \sum_{\mathbf{p}+\mathbf{q}=\mathbf{k}} u_\beta^{(\mathbb{P},\mathbb{Q})}(\mathbf{p},t) u_\gamma^{(\mathbb{P},\mathbb{Q})}(\mathbf{q},t), \tag{19}$$

where the sum is over all triads with $\mathbf{p} \in \mathbb{P}$ and $\mathbf{q} \in \mathbb{Q}$ such that $\mathbf{p}+\mathbf{q}=\mathbf{k}$.

For a statistically isotropic, homogeneous turbulence it is convenient to average over spherical shells in wave-vector space. In addition, in view of the considerable computational effort involved in computing all interactions between the very large number of scales present in the flow, we introduced a slight coarse graining in terms of the regions $\mathbb{P}$ and $\mathbb{Q}$ as shown in Fig. 2. Specifically, it was found adequate to group together contributions from four adjacent shells. Other more coarse "groupings" of wave numbers have been considered in the literature with the aim of extracting the dominant interaction processes at a reasonable computational effort. As an example a "logarithmic" grouping was adopted in Ref. [16] combining contributions from bands with a width of 2^k. In this paper we will look at the interactions of four shells $\mathbb{P}$ at distance k_p (cf. Fig. 2) with four shells $\mathbb{Q}$ at distance k_q that contribute to the nonlinear energy transfer to shell $\mathbb{S}_k$ characterized by the wave number k.

In terms of the transfer function $T_{\mathbb{PQ}}(\mathbf{k},t)$ we may now define the required spectral transfer functions. The energy transfer term (17) gives the exchange of energy by the triad $(\mathbf{k},\mathbf{p},\mathbf{q})$ where the latter two wave vectors are specified by the sets $\mathbb{P}$ and $\mathbb{Q}$ and the triangle constraint. Summing over all modes $\mathbf{k}$ in shell $\mathbb{S}_k$ we obtain the exact exchange of energy in the kth shell between k, k_p, and k_q:

$$T_{pq}(k,k_p,k_q,t) = \sum_{\mathbf{k}\in\mathbb{S}_k} T_{\mathbb{PQ}}(\mathbf{k},t). \tag{20}$$

We refer to T_{pq} as the "three-mode" transfer. The total energy transfer function $T(k,t)$ can be computed directly from Eq. (6) or as sum of the contributions from Eq. (20):

$$T(k,t) = \sum_{k_p} T_p(k,k_p,t), \tag{21}$$

in which the "two-mode" transfer T_p is given by

$$T_p(k,k_p,t) = \sum_{k_q} T_{pq}(k,k_p,k_q,t). \tag{22}$$

The individual transfer terms $T(k,t)$, $T_p(k,k_p,t)$, and $T_{pq}(k,k_p,k_q,t)$ give, respectively, more detailed characteristics of the energy transfer. The total transfer $T(k,t)$ expresses the amount of energy transferred from (negative) or to (positive) shell $\mathbb{S}_k$. All three transfer terms T, T_p, and T_{pq} will be used to investigate the transfer of energy in the sequel.

D. Simulation details

The numerical integration of the Navier-Stokes equations (1) is done via a four-stage, second-order, compact-storage, Runge-Kutta method [35]. To fully remove the aliasing error we applied a method that employs two shifted grids and spherical truncation [36]. We consider the canonical problem of forced turbulence in a cubic box of side L_b with periodic boundary conditions. Direct numerical simulations are characterized by N^3 computational points, where N is the number of grid points used in each direction. A detailed description of the simulation setup and the validation of the numerical procedure can be found in Ref. [21]. The components of the wave vector $\mathbf{k}$ are $k_\alpha=(2\pi/L_b)n_\alpha$ where $n_\alpha=0,\pm1,\pm2,\ldots,\pm(N/2-1),-N/2$for $\alpha=1,2,3$. The numerical simulations are defined further by the size of the domain ($L_b=1$), the computational Reynolds number Re, and the energy injection rates to the two distinct bands $(\varepsilon_{w,1},\varepsilon_{w,2})$.

We will study this homogeneous turbulent flow at two different computational Reynolds numbers, i.e., Re=1061 and Re=4243. In case of homogeneous, decaying turbulence these Reynolds numbers correspond to $R_\lambda=50$ or 100, in terms of the initial Taylor-Reynolds number [21]. The large-scale forcing of $\mathbb{S}_1$ has an energy injection rate $\varepsilon_{w,1}=0.15$ that is used as a reference case. For all simulations the fractal dimension was kept constant and equal to $D_f=2.6$ [27].

The smallest length scale that should be accurately resolved depends on the size of the box, viscous dissipation, and energy injection rate. Usually it is required that $k_{\max}\eta > 1$ [5,37,38] in terms of the Kolmogorov length scale η and the maximal magnitude of the wave vector $k_{\max}=\pi N/L_b$ that enters the computations. In our simulations $k_{\max}\eta \gtrapprox 2$ indicating that the small scales are well resolved.

We consider time-averaged properties of the turbulent flow. For a function h these are defined by

$$\langle h \rangle_t = \lim_{t\to\infty} \frac{1}{t-t_0}\int_{t_0}^{t} h(\tau)d\tau \approx \frac{1}{\mathcal{T}-t_0}\int_{t_0}^{\mathcal{T}} h(\tau)d\tau, \tag{23}$$

where $\mathcal{T}$ is sufficiently large. We start the averaging at $t_0=5$ which corresponds to about 10 eddy-turnover times for the simulated cases. The final time was taken equal to $\mathcal{T}=30$, so all results are averaged over approximately 50 eddy-turnover times. The accuracy of this approximation to the long-time average, measured as the ratio of the standard deviation and the mean signal, is less than 5% for all investigated quantities.

The energy spectra presented in this paper are shell and time averaged. Moreover, we focus on compensated spectra

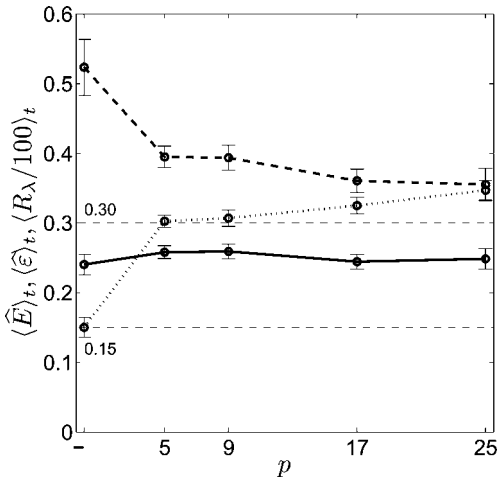

FIG. 3. Time-averaged total kinetic energy $\hat{E}$ (solid), total energy dissipation rate $\hat{\varepsilon}$ (dotted), and Taylor-Reynolds number R_λ (dashed) for forced turbulence with different locations of the second band at Re=1061.

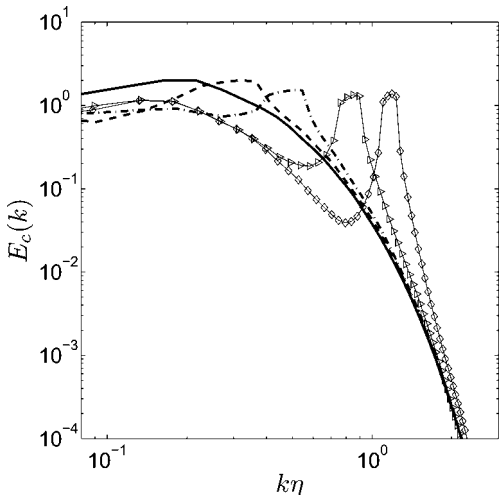

FIG. 4. Compensated shell- and time-averaged energy spectrum $E_c(k)$ for two-band forcing: $\mathbb{S}_1$ and $\mathbb{K}_{p,p+3}$. Large-scale forcing $\mathbb{S}_1$ (solid), additional forcing in the second band $\mathbb{K}_{5,8}$ (dashed), $\mathbb{K}_{9,12}$ (dash-dotted), $\mathbb{K}_{17,20}$ ($\triangleright$), $\mathbb{K}_{25,28}$ ($\diamond$) at Re=1061.

E_c in which we use nondimensional Kolmogorov units: $E_c(k)=\langle\hat{\varepsilon}\rangle_t^{-2/3}k^{5/3}\langle E_s(k,t)\rangle_t$ in terms of the shell-averaged spectrum $E_s(k,t)=\Sigma_{\mathbf{k}\in\mathbb{S}_k}E(\mathbf{k},t)$. The compensation of the spectrum is not strictly required to observe the characteristic changes in the energy distribution, but as it gives more information about the dominant scales present in a flow, it will be used throughout.

III. BROADBAND FORCED TURBULENCE

A. Energy distribution in forced turbulence

We first concentrate on the application of the high-k forcing band at *different locations* in spectral space. We apply a constant energy input rate $\varepsilon_{w,2}=0.15$ to this band. Simultaneously, the large-scale forcing to the first shell $\mathbb{S}_1$ is $\varepsilon_{w,1}=0.15$. The computational Reynolds number is Re=1061. We forced the bands $\mathbb{K}_{p,p+3}$ for $p=5$, 9, 17, 25. The parameters of these simulations with some of the statistics are further presented in the Appendix (runs 1 and 14–17 in Tables I and II are concerned here).

The total kinetic energy, energy dissipation rate, and Taylor-Reynolds number are shown in Fig. 3 as a function of the location of the left boundary p of the high-k forced band $\mathbb{K}_{p,p+3}$. The first data point refers to the classical large-scale forcing only (run 1). Application of broadband forcing in the different bands changes the characteristics of the flow modifying primarily the amount of small scales. This forcing in the second band is seen to increase the energy dissipation in the system. The Kolmogorov dissipation scale and the Taylor-Reynolds number decrease, suggesting that the characteristic scale at which dissipation plays an important role is shifted to smaller scales. We notice that the total energy in the system is only slightly affected by the introduction of forcing. Moving the broadband forcing to very small scales implies that there is no longer a strong influence on the flow because the energy injected in the small scales appears to be also dissipated immediately.

The compensated, shell-, and time-averaged energy spectrum for different locations of the forced region $\mathbb{K}_{p,p+3}$ are shown in Fig. 4. We may observe that the forcing causes a nonlocal depletion in the energy spectrum for the larger scales, while the tail of the spectrum is less affected. The pileup in the energy spectrum near the forcing region is characteristic of the explicit high-k forcing and is suggestive of a "blocking" or reverse cascading. If the separation between $\mathbb{S}_1$ and the high-k band is reduced, then the interaction is stronger and a considerable depletion of the energy levels in the largest scales arises. This is in agreement with the large-scale forced turbulence results, where the local and nonlocal interactions were found to be energetically dominant, while the distant interactions were mainly responsible for transferring structural information [30].

An effective modulation of turbulent quantities is possible not only by a change in the range of forced modes but also via a change in the energy input rate. To investigate this we adopted an energy injection rate $\varepsilon_{w,1}=0.15$ for the large-scale forcing in $\mathbb{S}_1$ and we vary the intensity of forcing in the second band by changing $\varepsilon_{w,2}$. We adopted the following values for $\varepsilon_{w,2}$: 0.07, 0.15, 0.30, 0.45, 0.60, 0.75, or 0.90 and considered forcing of four or eight shells in $\mathbb{K}_{17,20}$ or $\mathbb{K}_{17,24}$, respectively. The parameters and characteristic quantities can be found in Tables I and II as runs 2–7 and 8–13.

The total energy in the system is only slightly affected by the forcing strength in the second band as shown in Fig. 5. An increased forcing strength introduces additional energy into the flow at small scales that is dissipated very efficiently. This is expressed by the linear increase in $\langle\hat{\varepsilon}\rangle_t$. In Fig. 6 we present the compensated energy spectrum for various strengths of the forcing $\varepsilon_{w,2}$. The energy in the forced region reaches higher values with increasing $\varepsilon_{w,2}$. Changing the strength of the broadband forcing induces a characteristic depletion in the larger scales. This suggests that the additional forcing term enhances the nonlinear interactions, which influence various scales quite far away from the forced region. The energy that is injected at the larger scales

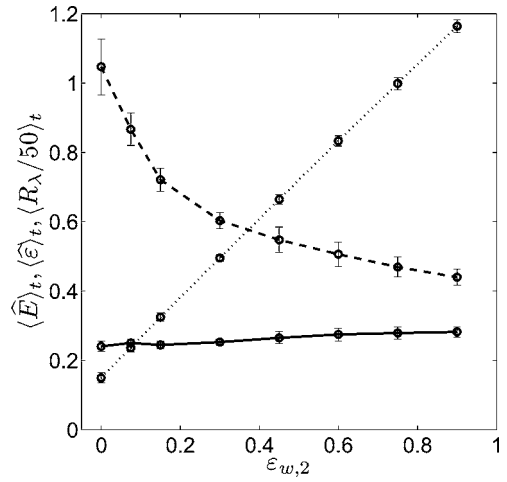

FIG. 5. Time-averaged total energy $\hat{E}$ (solid), total energy dissipation rate $\hat{\varepsilon}$ (dotted), and Taylor-Reynolds number R_λ (dashed) for two-band forced turbulence with varying strength in the second band $\varepsilon_{w,2}$ at Re=1061.

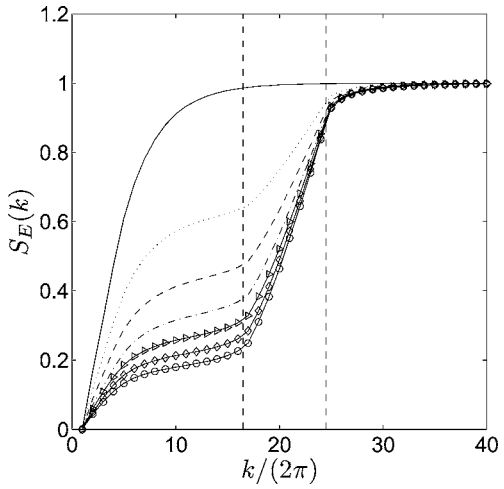

FIG. 7. Normalized accumulated energy $S_E(k)$ for two-band $\mathbb{S}_1$ and $\mathbb{K}_{17,24}$ forced turbulence at Re=1061. Large-scale forcing at $\varepsilon_{w,1}=0.15$ (solid) with additional second band forcing at $\varepsilon_{w,2}=0.15$, 0.30, 0.45, 0.60, 0.75, 0.90 is denoted by the dotted, dashed, dash-dotted, ▷, ◇, and ○ curves, respectively.

is transferred even more effectively through the cascade as $\varepsilon_{w,2}$ increases. This effect appears similar to the so-called spectral shortcut observed in nature and experiments [25]. In the case of such a shortcut the energy from larger scales is diverted quite directly to fine scales, largely bypassing the traditional cascading. This mechanism was explained in the case of flow over forest canopies in Ref. [25]. We will investigate it in more detail in the next section.

A final quantification of the nonlocal effect on the spectrum that arises from the high-k forcing is collected in Fig. 7. Here we displayed the normalized accumulated energy

$$S_E(k) = \frac{\sum_{k' \leqslant k} E_c(k')}{\sum_k E_c(k)} \tag{24}$$

in the consecutive shells. As pointed out, varying the properties of a flow in a specified spectral region can change the behavior of a flow well outside this region. In terms of $S_E(k)$ we notice that close to 90% of the energy is present in the first ten shells (Fig. 7) when only the large-scale forcing is applied. Influencing the flow at smaller scales in $\mathbb{K}_{17,24}$ is seen to remove most of the energy from these larger scales while there is only a slight impact on the dynamics of small scales. This effect becomes more pronounced with increasing $\varepsilon_{w,2}$. The underlying changes in the energy transfer will be considered in more detail in Sec. IV.

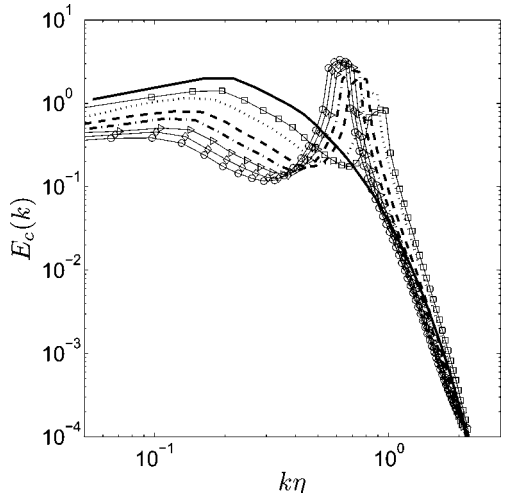

FIG. 6. Compensated shell- and time-averaged energy spectrum $E_c(k)$ for forced turbulence in the band $\mathbb{K}_{17,20}$ at different strengths of forcing $\varepsilon_{w,2}$ and Re=1061. Large-scale forcing only (solid), additional second band forcing with $\varepsilon_{w,2}=0.07$, 0.15, 0.30, 0.45, 0.60, 0.75, 0.90 denoted as □, dotted, dashed, dash-dotted, ▷, ◇, ○, respectively. In each case $\varepsilon_{w,1}=0.15$.

B. Energy transfer spectra

The transfer of energy in turbulence can be described in spectral space as interactions of triads of wave vectors $(\mathbf{k},\mathbf{p},\mathbf{q})$ that form triangles, i.e., $\mathbf{k}=\mathbf{p}+\mathbf{q}$. Direct numerical simulation with large-scale forcing shows that nonlocal interactions between wave vectors combine into a local energy flow [13,31]. By applying forcing that is located in a high-k range of spectral space we perturb the "natural" cascading process. The associated changes in the transfer of energy will be investigated in more detail in this subsection. Specifically, we focus on the energy transfer and energy transport power spectra.

In large-scale forced turbulence energy is injected into the first shell and removed by the transfer term. This gives rise to negative values, for the energy transfer in the forced region. In the higher shells the transfer function takes on positive values which illustrates the transfer of energy through the cascade toward higher k. By invoking the broadband forcing we influence this basic energy cascade. This is clearly seen in the energy transfer spectrum which develops distinctive re-

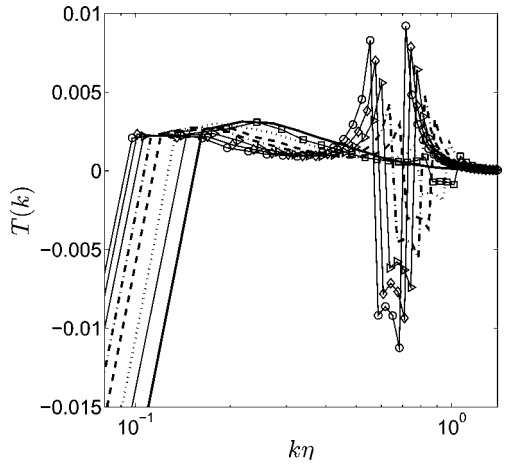

FIG. 8. Time-averaged energy transfer $T(k)$ for two-band $\mathbb{S}_1$ and $\mathbb{K}_{17,20}$ forced turbulence for different strengths of forcing in the second band $\varepsilon_{w,2}$ at Re=1061. Large-scale forcing (solid) with additional second band forcing at $\varepsilon_{w,2}$=0.07, 0.15, 0.30, 0.45, 0.60, 0.75, 0.90 denoted by □, dotted, dashed, dash-dotted, ▷, ◇, and ○ curves, respectively.

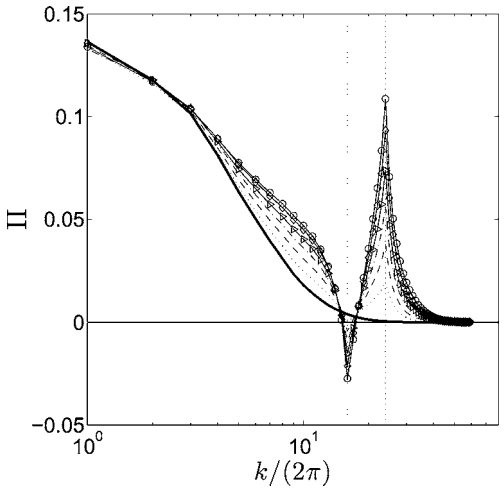

FIG. 9. Time-averaged transport power spectra for broadband forced turbulence in the $\mathbb{K}_{17,24}$ band at Re=1061. Large-scale forcing (solid) with additional second band forced at $\varepsilon_{w,2}$=0.15, 0.30, 0.45, 0.60, 0.75, 0.90 denoted as dotted, dashed, dash-dotted, ▷, ◇, ○, curves, respectively. The supplementary forced region $k_1 < k \leq k_2$ is denoted with dotted lines.

gions where $T(k)=\langle T(k,t)\rangle_t$ is negative. Figure 8 characterizes changes in the transfer function due to an increased forcing strength of the high-k band. The transfer function reaches lower values between the low- and high-k forcing regions compared to the large-scale forced case. The reverse situation appears near the high-k forced band where the transfer increases with an increase of the forcing intensity. This is in agreement with the energy spectra presented earlier, where we observed the depletion of energy between the forced regions. This effect can be observed more directly from spectra of energy transport power that will be presented next.

The energy transport power gives the rate at which energy is transferred from shells $k' < k$ to those with $k' > k$:

$$\Pi(k,t) = \int_k^{k_{\max}} T(k',t)dk' = -\int_0^k T(k',t)dk', \qquad (25)$$

where $k_{\max}=\pi N/L_b$ is the cutoff wave number. We present the time-averaged transport power spectrum $\Pi(k)=\langle\Pi(k,t)\rangle_t$ in Fig. 9 for forcing with various strengths in the $\mathbb{K}_{17,24}$ band. In case of large-scale forcing only, the transport power is positive for all k as the energy is transferred toward smaller scales and reaches zero for large k indicating the general property of the total transfer function $\hat{T}(t)=0$. The application of high-k forcing for $k_1 < k \leq k_2$ changes this well-known picture. First, we note that the values of the transport power are all similar in the largest scales, where the flow is governed by the same energy input. The transport power for $0 < k \leq k_1$ becomes larger at higher $\varepsilon_{w,2}$. A striking change of the behavior arises for k near and inside the high-k forced region. The transport power spectrum even assumes negative values for $k \approx k_1$.

The observed behavior of the transport power in Fig. 9 is partly due to the relatively low Reynolds number that was used. At sufficiently high Reynolds numbers, the dissipation scales are much more separated from the high-k forced scales. In this case a plateau of Π will arise at low wave numbers: $\Pi(k,t) \approx \varepsilon_{w,1}$ for k low enough [1]. This property is not observed at the computational Reynolds number considered so far.

In cases specified by runs 18 and 19 we consider the flow at a four times higher computational Reynolds number. The overall results for the energy spectra and energy transfer were found to be qualitatively the same as in the lower Reynolds number cases. However, a plateau may now be observed in Fig. 10, where we present the transport power for the higher Reynolds number. In this case the transport power does not decrease below zero in the forced region. The second forcing band is well separated from the dissipation re-

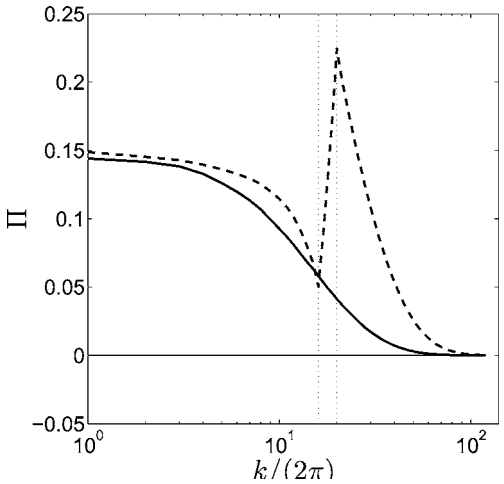

FIG. 10. Time-averaged transport power spectra for Reynolds number Re=4243 and forcing in the $\mathbb{K}_{17,20}$ band. Large-scale forcing (solid), additional broadband forcing in the $\mathbb{K}_{17,20}$ band with $\varepsilon_{w,2}$=0.30 (dashed).

gion and the transport power in this band is much larger, approaching a maximum 0.23 that is near the energy injection rate $\varepsilon_{w,2}$.

In this section we have looked at the effect of high-k modulation of the energy cascading process that leads to an increased energy dissipation in small scales. This process is supported by an increased energy transfer to smaller scales via nonlocal triad interactions. The effect of increased energy rate by the application of broadband forcing is seen in the energy transfer and transport power spectra. In the next section we will look more closely at the interactions of various scales of motion under the influence of broadband forcing by considering the two- and three-mode transfers T_p and T_{pq} introduced in Eqs. (22) and (20).

IV. TWO- AND THREE-MODE INTERACTION OF SCALES

The energy dynamics of turbulent flow is generally discussed in terms of the transfer of kinetic energy from larger to smaller scales through nonlinear interactions. The statistical properties of turbulence are determined by these interactions. In the previous section we have shown how additional broadband forcing of inertial range scales can modify the classical picture of the Kolmogorov cascade. To investigate the observed turbulence modulation effects in more detail we consider the underlying two- and three-mode energy transfer terms in this section. This will clarify to some extent the changes in the various nonlinear interactions that give rise to the observed alterations in the spectra and energy transfer.

We start with the three-mode transfer that is averaged in time $T_{pq}(k,k_p,k_q)=\langle T_{pq}(k,k_p,k_q,t)\rangle_t$ and split this term into its positive and negative parts:

$$T_{pq}(k,k_p,k_q) = T^-_{pq}(k,k_p,k_q) + T^+_{pq}(k,k_p,k_q), \tag{26}$$

in which

$$T^+_{pq}(k,k_p,k_q) = \begin{cases} T_{pq}(k,k_p,k_q) & \text{if } T_{pq}(k,k_p,k_q) \geq 0, \\ 0 & \text{otherwise}, \end{cases} \tag{27}$$

with a similar definition for the negative part:

$$T^-_{pq}(k,k_p,k_q) = \begin{cases} T_{pq}(k,k_p,k_q) & \text{if } T_{pq}(k,k_p,k_q) < 0, \\ 0 & \text{otherwise}. \end{cases} \tag{28}$$

In terms of these contributions we examine the normalized triad energy transfer

$$\bar{T}_{pq}(k,k_p,k_q) = \frac{T^-_{pq}(k,k_p,k_q)}{T_{\min}(k)} + \frac{T^+_{pq}(k,k_p,k_q)}{T_{\max}(k)}, \tag{29}$$

where

$$T_{\min}(k) = -\min_{k_p,k_q}(T^-_{pq}(k,k_p,k_q)),$$

$$T_{\max}(k) = \max_{k_p,k_q}(T^+_{pq}(k,k_p,k_q)). \tag{30}$$

Through the scaling of T^-_{pq} and T^+_{pq} with $T_{\min}$ and $T_{\max}$, respectively, the normalized transfer is well suited to characterize the overall structure of the three-mode transfer function, even in cases in which the order of magnitude of T_{pq} varies considerably. The normalized energy transfer $\bar{T}_{pq}(k,k_p,k_q)$ is plotted in Fig. 11 for three different wave numbers $k/(2\pi)=14$, 42, 82, based on run 19 in which $R_\lambda \cong 75$. The three k values that are selected correspond to wave numbers below the forced region $[k/(2\pi)=14]$ or to wave numbers that are considerably larger. Such contour maps for $\bar{T}_{pq}$ can also be found in Ref. [19] for the case of large-scale forced turbulence. For completeness, we also presented the results from such large-scale forced turbulence (run 18) comparing these directly to the broadband forced turbulence (run 19). This contour map is shown in Fig. 12 for $k/(2\pi)=46$.

The strongest interactions are observed for modes with wave numbers between the largest forced scales and the high-k forced region as can be seen in Fig. 11(a). As in the case of large-scale forcing only we observe very strong interactions between Fourier modes of considerably different scales. These are located in the corners of the rectangular domains in the k_p-k_q plane. Distant interactions are well separated from the origin in these figures. Their contribution to the transfer is seen to be very small, as also noticed earlier in the literature [19]. The change of sign in the transfer function that occurs at $k_p=k$ and $k_q=k$, respectively, on the k_p-k_q planes indicates that in this region the energy is mainly transferred to higher k.

The most efficient transfer takes place between two wave vectors of similar size and one of quite different size as seen in the corners of the rectangular area in Fig. 11. This is in agreement with previous numerical experiments reported by various authors [2,16,19]. However, compared to the case of large-scale forcing only, we now observe quite extended, highly energetic interactions with the high-k forced region. The second forced band causes regions with high intensity of interactions to be much wider compared to the case of large-scale forcing only. This is visible directly in Fig. 12. The regions with positive and negative transfer are extended from the corners to the wave-number regions where the actual application of forcing in the second band occurs. The energy is exchanged predominantly between scales that are more separated than in case of the large-scale forced flow where the dominant interactions occur only in the corners. This is a clear indication of the stronger nonlocal interactions, mentioned earlier.

For further clarification of energy transfer processes we turn to the time-averaged two-mode energy transfer $T_p(k,k_p)=\langle T_p(k,k_p)\rangle_t$, which gives information about the interactions involving a sum over all k_q wave numbers at fixed k and k_p. The sum involves all k_q wave numbers that are constrained by the triadic interactions, i.e., their length may vary between $|\mathbf{k}-\mathbf{p}|$ and $|\mathbf{k}+\mathbf{p}|$. We normalized the two-mode transfer function $T_p(k,k_p)$ in a similar manner as $T_p(k,k_p,k_q)$:

$$\bar{T}_p(k,k_p) = \frac{T^-_p(k,k_p)}{T_{\min}(k)} + \frac{T^+_p(k,k_p)}{T_{\max}(k)}, \tag{31}$$

where $T^\pm_p$, $T_{\min}$, and $T_{\max}$ are defined in terms of T_p in a manner analogous to the definitions in Eqs. (26)–(28) and

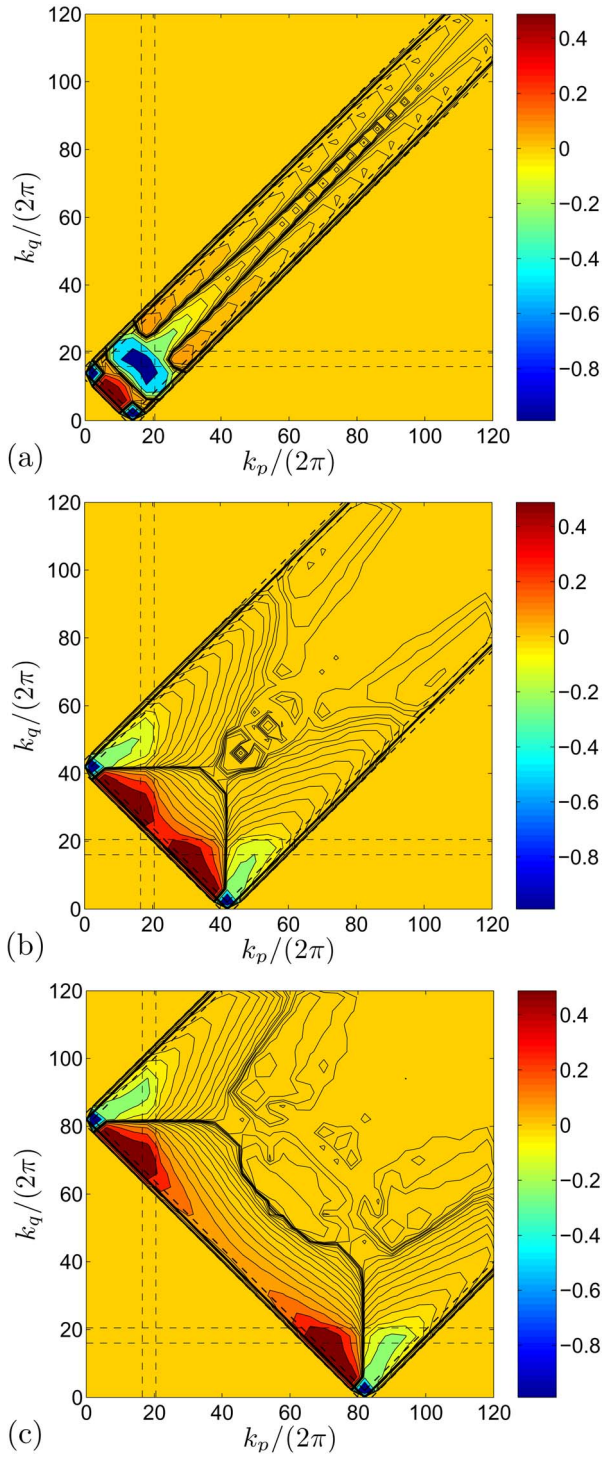

FIG. 11. (Color online) The normalized triad energy transfer function $\bar{T}_{pq}(k,k_p,k_q)$ for $k/(2\pi)=14$, 42, 82 in (a)–(c), respectively. The dashed lines correspond to the lower (k_1) and upper (k_2) wave numbers used in the broadband forcing at Re=4243. The contour levels are $\pm 1/2^n$, $n=0,\ldots,18$ that are the same for all three pictures.

(30). In Fig. 13 we plotted the contour map of $\bar{T}_p(k,k_p)$. For larger wave numbers this quantity was found to look quite similar to the case of large-scale forced turbulence. The two-mode transfer function changes sign from negative to positive at $k=k_p$, indicating a downward energy flow. Comparing this to the large-scale forced turbulence we observe (i) strong influence of forcing in the regions where it is applied (denoted with dashed lines), (ii) extended negative energy transfer region with comparatively high magnitude above the $k=k_p$ line, (iii) amplification of the backward energy transfer indicated by the positive region for small k and large k_p. This region is separated from the intense negative energy transfer region by the indicated accumulation of contour lines above the $k=k_p$ line appearing as the curved black line.

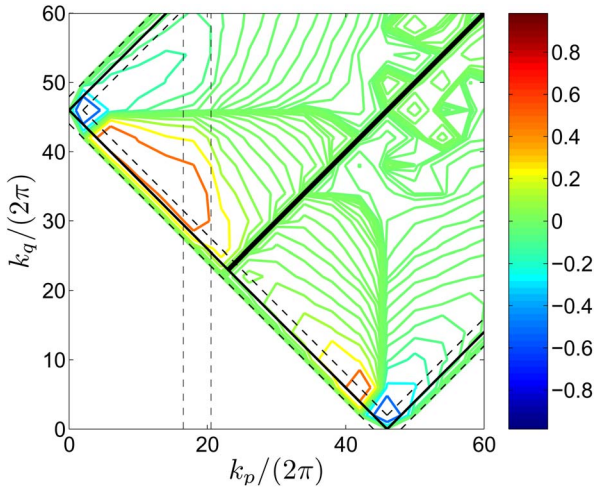

FIG. 12. (Color online) The normalized triad energy transfer function $\bar{T}_{pq}(k,k_p,k_q)$ for $k/(2\pi)=46$ at Re=4243. The upper (bottom) rectangle presents broadband (large-scale) forced turbulence, respectively. The contour levels are $\pm 1/2^n$, $n=0,\ldots,24$.

A more quantitative overview is plotted in Fig. 14 displaying the two-mode transfer function in the range $k_p/(2\pi)=30,34,\ldots,94$. This clearly shows the cascading character of the energy flow from larger to smaller scales in the system. The modification due to the high-k forcing expresses itself by the sequence of one slightly positive, two

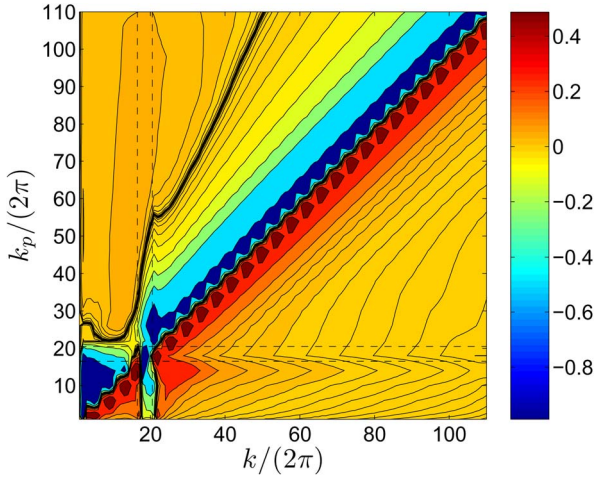

FIG. 13. (Color online) The normalized triad energy transfer function $\bar{T}_p(k,k_p)$ at Re=4243 (run 19). The contour levels are $\pm 1/2^n$, $n=0,\ldots,18$. The supplementary forced region $k_1<k\leq k_2$ denoted with dashed lines.

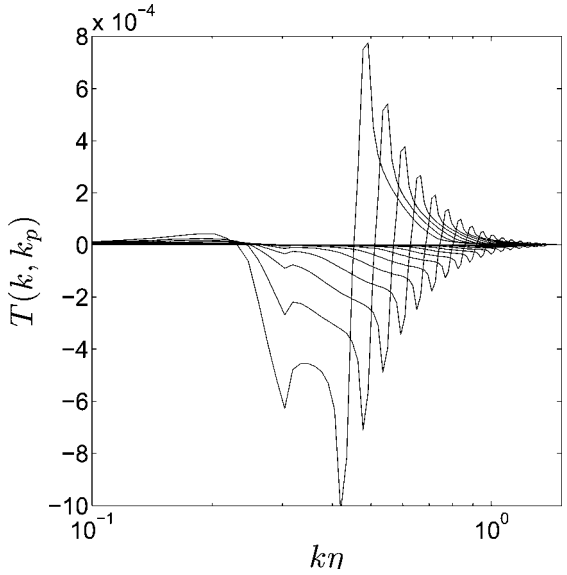

FIG. 14. The triad energy transfer function $T_p(k,k_p)$ at $k_p/(2\pi)=30,34,\ldots,94$ and Re=4243 (run 19).

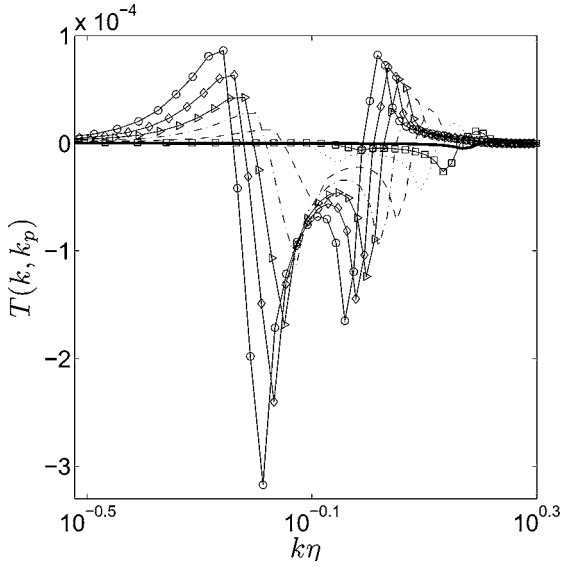

FIG. 15. The triad energy transfer function $T_p(k,k_p)$ at $k_p/(2\pi)=30$ and Re=1061. Large-scale forcing (solid) with additional second band forced at $\varepsilon_{w,2}=0.07$, 0.15, 0.30, 0.45, 0.60, 0.75, 0.90 denoted as □, dotted, dashed, dash-dotted, ▷, ◇, ○, respectively.

quite negative and one quite positive local extrema. The intensity of the energy transfer decreases with increasing wave numbers as less energy needs to be transferred. This corresponds directly to the magnitude of $T_{\min}(k)$ and $T_{\max}(k)$ used in the normalization of $T_p(k,k_p)$ [Eq. (31)]. The part in which the transfer is negative is much wider in the broadband forced case compared to the large-scale forced turbulence results.

We conclude by considering the effect of varying the forcing strength $\varepsilon_{w,2}$ at a characteristic wave number $k_p/(2\pi)=30$ on the two-mode energy transfer function $T_p(k,k_p)$. This is shown in Fig. 15. In the large-scale forced case at $\varepsilon_{w,2}=0$ the transfer is very small compared to the cases in which the high-k forcing is active. In addition, the effect is very localized (solid line in Fig. 15). The forcing in the high-k band completely changes this behavior. The intensity of the energy transfer is directly related to the value of $\varepsilon_{w,2}$. Additional extrema appear in the two-mode transfer function. The high-k forced cases display two pairs in which a negative minimum is combined with a positive maximum, while large scale forcing only yields one such combination. Correspondingly, the min-max pair at high k is associated with the large scale forcing in S_1 while the min-max pair at lower k originates from the additional forcing in the second band. We also investigated three-band forcing and observed further peaks in the energy transfer spectra.

V. CONCLUDING REMARKS

We performed direct numerical simulations of broadband forced turbulence to explore accumulated effects on the time-averaged energy transfer in isotropic homogeneous turbulence. Using broadband forcing based on a recently proposed mathematical model for a fractal stirrer [27] we have shown how the application of such forcing modulates turbulence both qualitatively and quantitatively. The modulation is similar to that observed in experiments based on flows through porous media or canopies. Specifically the perturbation of a flow arising from the contact with complex physical boundaries enhances the dissipation and causes an abrupt energy drain from large to small scales. This aspect of simultaneous perturbation of a flow on a spectrum of length scales is retained in the cases studied here.

We found that broadband forcing that perturbs a turbulent flow at smaller scales enhances nonlocal triad interactions and alters the detailed cancellation processes that occur in the traditional large-scale forced flows. This leads to nonlocal modifications in the energy transfer spectrum and the energy distribution among scales. We verified this by partitioning the nonlinear term in the Navier-Stokes equations in terms of different triad contributions to the total transfer function. The energy transport power is found to be enhanced in the spectral region in between the large-scale and the high-k forced bands. This characteristic may be influenced via the control parameters of the applied forcing, i.e., its strength and extent of agitated scales, and allows optimizing transport processes of turbulent flows.

Future study will involve the examination of the consequences of forcing in the physical space context. We will investigate the geometrical statistics of broadband forced turbulence looking at the interactions of strain and vorticity and their modulation by the applied forcing. This may help understanding which physical processes are responsible for the observed modulations and how to exploit this to enhance physical space mixing.

ACKNOWLEDGMENTS

This work is part of the research program "Turbulence and its role in energy conversion processes" of the Founda-

TABLE I. Direct numerical simulation parameters using a resolution of $N=128$ and $\mathrm{Re}=1061$ in runs 1–17, and a resolution of $N=256$ at $\mathrm{Re}=4243$ in runs 18 and 19. The cases with large-scale forcing only are denoted by $\star$. In this table ε_w denotes the energy input rate in the high-k band, except runs 1 and 18 in which it corresponds to the energy input rate in $\mathbb{S}_1$. Moreover, m and p characterize the spectral support of the high-k band $\mathbb{K}_{m,p}$.

Run	ε_w	m	p	Run	ε_w	m	p
1	$0.15^\star$						
2	0.07	17	20	8	0.15	17	24
3	0.30	17	20	9	0.30	17	24
4	0.45	17	20	10	0.45	17	24
5	0.60	17	20	11	0.60	17	24
6	0.75	17	20	12	0.75	17	24
7	0.90	17	20	13	0.90	17	24
14	0.15	5	8	18	$0.15^\star$		
15	0.15	9	12	19	0.30	17	20
16	0.15	17	20				
17	0.15	25	28				

tion for Fundamental Research of Matter (FOM). The authors wish to thank NCF (Dutch Foundation for National Computing Facilities) for supporting the computations. These were executed at SARA Computing and Networking Services in Amsterdam.

APPENDIX

The main parameters of the simulations are collected in Table I. The corresponding statistics of the velocity fields are summarized in Table II. The quantities compiled in Table II are the Kolmogorov dissipation wave number k_d, which is the inverse of the Kolmogorov length scale η, the product $k_{\max}\eta$, the Taylor microscale $\lambda=[5\hat{E}/\Sigma_{\mathbf{k}}k^2E(\mathbf{k},t)]^{1/2}$, the Taylor-microscale Reynolds number $R_\lambda=\lambda u'/\nu$, the integral length scale $L=3\pi/(4\hat{E})\Sigma_{\mathbf{k}}k^{-1}E(\mathbf{k},t)$, the integral Reynolds number $R_L=Lu'/\nu$, the rms velocity $u'=(2\hat{E}/3)^{1/2}$, the energy dissipation rate $\varepsilon=\Sigma_{\mathbf{k}}2\nu k^2E(\mathbf{k},t)$, the eddy-turnover time $\tau=L/u'$, and the skewness $S=2/35(\lambda/u')^3\Sigma_{\mathbf{k}}k^2T(\mathbf{k},t)$. All these quantities in Table II are time averaged $\langle\cdot\rangle_t$ as described in Sec. II D.

We also checked that the alteration of the cascading process caused by the high-k forcing does not influence the isotropy of the flow field. A measure of isotropy was suggested in Ref. [39] given by $I^2(t)=\psi_1(t)/\psi_2(t)$ where $\psi_1(t)=\langle|\mathbf{e}_1(\mathbf{k})\mathbf{u}(\mathbf{k},t)|^2\rangle$, $\psi_2(k,t)=\langle|\mathbf{e}_2(\mathbf{k})\mathbf{u}(\mathbf{k},t)|^2\rangle$ are the kinetic energy along the components of two orthogonal solenoidal unit vectors $\mathbf{e}_1(\mathbf{k})=\mathbf{k}\times\mathbf{z}(\mathbf{k})/|\mathbf{k}\times\mathbf{z}(\mathbf{k})|$, $\mathbf{e}_2(\mathbf{k})=\mathbf{k}\times\mathbf{e}_1(\mathbf{k})/|\mathbf{k}\times\mathbf{e}_1(\mathbf{k})|$ where $\mathbf{z}(\mathbf{k})$ is a randomly oriented unit vector. The operator $\langle\cdot\rangle$ denotes averaging over these random unit vectors. For isotropic turbulence one can expect to find $I=1$, i.e., $\psi_1=\psi_2$ which was confirmed to close approximation in all simulations. Deviations from the expected value for I were found to be of the order of 1%.

TABLE II. Direct numerical simulations statistics of the different cases studied.

Run	k_d	$k_{\max}\eta$	λ	R_λ	L	R_L	u'	ε	τ	S
1	116	3.26	0.123	52	0.23	97	0.40	0.15	0.57	0.49
2	130	2.91	0.100	43	0.23	100	0.41	0.24	0.56	0.35
3	156	2.42	0.069	30	0.23	98	0.41	0.50	0.54	0.21
4	168	2.25	0.061	27	0.23	101	0.42	0.66	0.54	0.17
5	178	2.12	0.056	25	0.22	102	0.43	0.83	0.52	0.15
6	186	2.03	0.051	23	0.22	102	0.43	1.00	0.52	0.14
7	193	1.95	0.048	22	0.22	100	0.43	1.16	0.50	0.13
8	140	2.68	0.085	37	0.23	99	0.41	0.33	0.56	0.29
9	156	2.41	0.070	31	0.23	102	0.41	0.50	0.56	0.22
10	169	2.24	0.060	26	0.22	98	0.41	0.68	0.54	0.18
11	178	2.11	0.054	24	0.22	100	0.42	0.85	0.53	0.16
12	187	2.02	0.049	22	0.22	97	0.42	1.03	0.52	0.15
13	194	1.94	0.046	21	0.21	96	0.42	1.20	0.50	0.13
14	138	2.73	0.090	39	0.22	96	0.41	0.30	0.52	0.44
15	138	2.72	0.089	39	0.23	102	0.42	0.31	0.56	0.39
16	140	2.69	0.084	36	0.22	96	0.40	0.33	0.55	0.28
17	143	2.64	0.082	36	0.23	98	0.41	0.35	0.56	0.22
18	325	2.32	0.065	115	0.21	368	0.42	0.15	0.50	0.51
19	432	1.74	0.040	75	0.21	394	0.44	0.46	0.47	0.38

[1] W. D. McComb, *The Physics of Fluid Turbulence* (Oxford University Press, New York, 1990).
[2] Y. Zhou and Ch. G. Speziale, Appl. Mech. Rev. **51**, 267 (1998).
[3] E. D. Siggia, J. Fluid Mech. **107**, 375 (1981).
[4] R. M. Kerr, J. Fluid Mech. **153**, 31 (1985).
[5] V. Eswaran and S. B. Pope, Comput. Fluids **16**, 257 (1988).
[6] S. Chen and X. Shan, Comput. Phys. **6**, 643 (1992).
[7] J. Jimenez, A. A. Wray, P. G. Saffman, and R. S. Rogallo, J. Fluid Mech. **255**, 65 (1993).
[8] S. Ghosal, T. S. Lund, P. Moin, and K. Akselvoll, J. Fluid Mech. **286**, 229 (1995).
[9] L. Machiels, Phys. Rev. Lett. **79**, 3411 (1997).
[10] M. R. Overholt and S. B. Pope, Comput. Fluids **27**, 11 (1998).
[11] Y. Kaneda, T. Ishihara, M. Yokokawa, K. Itakura, and A. Uno, Phys. Fluids **15**, L21 (2003).
[12] A. N. Kolmogorov, C. R. Acad. Sci. URSS **30**, 301 (1941).
[13] Y. Zhou, Phys. Fluids A **5**, 1092 (1993).
[14] J. A. Domaradzki, R. W. Metcalfe, R. S. Rogallo, and J. J. Riley, Phys. Rev. Lett. **58**, 547 (1987).
[15] J. A. Domaradzki, Phys. Fluids **31**, 2747 (1988).
[16] J. A. Domaradzki and R. S. Rogallo, Phys. Fluids A **2**, 413 (1990).
[17] J. A. Domaradzki, Phys. Fluids A **4**, 2037 (1992).
[18] J. A. Domaradzki, W. Lui, C. Hartel, and L. Kleiser, Phys. Fluids **6**, 1583 (1994).
[19] K. Ohkitani and S. Kida, Phys. Fluids A **4**, 794 (1992).
[20] F. Waleffe, Phys. Fluids A **4**, 350 (1992).
[21] A. K. Kuczaj and B. J. Geurts, J. Turbul. (to be published).
[22] W. D. McComb and K. T. J. Chan, Nature (London) **292**, 520 (1981).
[23] W. D. McComb and K. T. J. Chan, J. Fluid Mech. **152**, 455 (1985).
[24] K. Boomsma, D. Poulikakos, and F. Zwick, Mech. Mater. **35**, 1161 (2003).
[25] J. Finnigan, Annu. Rev. Fluid Mech. **32**, 519 (2000).
[26] A. Pouquet, U. Frisch, and J. P. Chollet, Phys. Fluids **26**, 877 (1983).
[27] B. Mazzi and J. C. Vassilicos, J. Fluid Mech. **502**, 65 (2004).
[28] B. Mazzi, F. Okkels, and J. C. Vassilicos, Eur. Phys. J. B **28**, 243 (2002).
[29] P. K. Yeung and J. G. Brasseur, Phys. Fluids A **3**, 884 (1991).
[30] J. G. Brasseur and Ch-H. Wei, Phys. Fluids **6**, 842 (1994).
[31] Y. Zhou, Phys. Fluids A **5**, 2511 (1993).
[32] Y. Zhou, P. K. Yeung, and J. G. Brasseur, Phys. Rev. E **53**, 1261 (1996).
[33] Y. Suzuki and Y. Nagano, Phys. Fluids **11**, 3499 (1999).
[34] P. Moin and T. Bewley, Appl. Mech. Rev. **47**, S3 (1994).
[35] B. J. Geurts, *Elements of Direct and Large-Eddy Simulation* (R. T. Edwards, Inc., Ann Arbor, 2004).
[36] C. Canuto, M. Hussaini, A. Quarteroni, and T. Zang, *Spectral Methods in Fluid Dynamics* (Springer-Verlag, Berlin and New York, 1988).
[37] P. K. Yeung, J. G. Brasseur, and Q. Wang, J. Fluid Mech. **283**, 43 (1995).
[38] W. D. McComb, A. Hunter, and C. Johnston, Phys. Fluids **13**, 2030 (2001).
[39] J. H. Curry, J. R. Herring, J. Loncaric, and S. A. Orszag, J. Fluid Mech. **147**, 1 (1984).